crystals

Article

Comprehensive Study and Optimization of Implementing p-NiO in β-Ga_2O_3 Based Diodes via TCAD Simulation

Hong Zhou, Shifan Zeng, Jincheng Zhang *, Zhihong Liu *, Qian Feng, Shengrui Xu, Jinfeng Zhang and Yue Hao

Key Laboratory of Wide Band Gap Semiconductor Materials and Devices, School of Microelectronics, Xidian University, Xi'an 710071, China; hongzhou@xidian.edu.cn (H.Z.); 19111212912@stu.xidian.edu.cn (S.Z.); qfeng@mail.xidian.edu.cn (Q.F.); srxu@xidian.edu.cn (S.X.); jfzhang@xidian.edu.cn (J.Z.); yhao@xidian.edu.cn (Y.H.)

* Correspondence: jchzhang@xidian.edu.cn (J.Z.); zhihong@xidian.edu.cn (Z.L.)

Abstract: In this paper, we carried out a comprehensive study and optimization of implementing p-NiO in the β-Ga_2O_3 based diodes, including Schottky barrier diode (SBD) with p-NiO guard ring (GR), p-NiO/β-Ga_2O_3 heterojunction (HJ) barrier Schottky (HJBS) diode, and HJ-PN diode through the TCAD simulation. In particular, we provide design guidelines for future p-NiO-related Ga_2O_3 diodes with material doping concentrations and dimensions to be taken into account. Although HJ-PN has a ~1 V higher turn-on voltage (V_{on}), its breakdown voltage (BV) is the highest among all diodes. We found that for SBD with p-NiO GRs and HJBS, their forward electrical characteristics and reverse leakage current are related to the total width and the doping concentration of p-NiO, the BV is only related to the doping concentration of p-NiO, and the optimal doping concentration of p-NiO is found to be 4×10^{17} cm^{-3}. Compared with the SBD without p-NiO, the BV of the SBD with p-NiO and HJBS diode can be essentially improved by 3 times. As a result, HJ-PN diode, SBD with p-NiO GRs, and HJ-BS diode achieve a BV/specific on-resistance ($R_{on,sp}$) of 5705 V/4.3 mΩ·cm^2, 3006 V/3.07 mΩ·cm^2, and 3004 V/3.06 mΩ·cm^2, respectively. Based on different application requirements, this work provides a useful insight about the diode selection with various structures.

Keywords: Ga_2O_3; NiO; diode; simulation; Schottky diodes; JBS; PN junction

Citation: Zhou, H.; Zeng, S.; Zhang, J.; Liu, Z.; Feng, Q.; Xu, S.; Zhang, J.; Hao, Y. Comprehensive Study and Optimization of Implementing p-NiO in β-Ga_2O_3 Based Diodes via TCAD Simulation. *Crystals* **2021**, *11*, 1186. https://doi.org/10.3390/cryst11101186

Academic Editors: Haiding Sun, Dmitri Donetski, Bharat Jalan, Shibing Long, Yuhao Zhang, Rajendra Singh, Xuelin Yang, Yuji Zhao and Bin Liu

Received: 15 August 2021
Accepted: 24 September 2021
Published: 29 September 2021

1. Introduction

Beta-phase Ga_2O_3 (β-Ga_2O_3) has attracted tremendous attention as a promising material for power electronic applications because of its excellent physical properties, such as wide energy band gap of 4.6–4.9 eV, estimated high critical breakdown electric field of 8 MV/cm, decent electron mobility of 250 cm^2/Vs with high electron saturation velocity of 2×10^7 cm/s, and the cost-effective substrate through melt-grown methodology [1–5]. As a beneficial result of the excellent material properties, the Baliga's figure of merit is yielded to be around 3000, which is several times higher than that value of SiC and GaN [6]. However, due to the challenge of acquiring p-type Ga_2O_3, most research attention is paid to unipolar devices, including both the lateral and vertical field effect transistors (FETs) and diodes [7–12]. In particular, vertical diodes are regarded as the most promising commercial available product within the next 2–3 years. Accordingly, a significant amount of research is invested in improving the diode performance and hence many advanced edge termination techniques are being developed, including implanted edge termination, field plate, and Fin-type trench structures. State-of-the-art Ga_2O_3 vertical diodes have acquired a BV of 2.89 kV and DC power figure of merit (P-FOM) of around 1 GW/cm^2, which are still far less than its theoretical values [13]. For the further development of Ga_2O_3, the implementation of p-type materials for PN junction termination is very important for wide band gap materials to alleviate the high field crowding effect at the anode edge. However, p-type Ga_2O_3 has been reported to be a bottleneck due to the difficulty in finding acceptor species with small activation energy. In addition, the calculated valence band structure is found to be extremely flat, leading to a large hole effective mass; subsequently, the holes can be regarded as polartons and even the acceptor can ionize holes [14,15].

A temporary solution to resolve the p-type issue is by applying other p-type semiconductors instead of p-type Ga_2O_3 to fabricate the HJ architecture. Recently, some preliminary studies have combined p-type oxides with n-Ga_2O_3 to construct HJPN diodes for high BV purposes [16–19]. Among those p-type semiconductors, NiO is a good alternative to p-type Ga_2O_3 owing to its wide energy band gap. NiO is a material with a rock salt crystal structure and its band gap value depends on the growth condition which is between 3.8 and 4.2 eV [20–22]. Further, values for its hole mobility between 0.12 and 0.94 cm^2/V s have been reported [17]. Although the NiO/Ga_2O_3 HJ diodes have been reported to improve the BV, the performance of those diodes is still far away from its ideal value and is facing significant material and device structure design challenges. For example, our recent work employed a HJ-JBS geometry to demonstrate a high P-FOM of 0.92 GW/cm^2, however its V_{on} was around 1.5~2 V, the BV was only 1.3 kV and the simulated peak electrical field was just 3.4 MV/cm [23]. Estimating the electrical theoretical limit of p-NiO/Ga_2O_3 HJ diodes is very important for exploring the potential of NiO as a replacement of p-type Ga_2O_3, which is missing in previous work. Moreover, the physical insights into the electrical field distribution in NiO/Ga_2O_3 HJ diodes have not been fully discussed. In order to fully explore the NiO/Ga_2O_3 based HJ diode potentials and address aforementioned concerns, we carried out a comprehensive study on the SBD without p-NiO, SBD with p-NiO GRs, HJBS diode with periodic p-NiO arrays, and HJ-PN diode by performing drift layer thickness and NiO doping concentration, as well as NiO width dependent electrostatics, forward and reverse characteristic simulations. By doing this, we hope that this article can provide some hints and guidelines for future NiO/Ga_2O_3 HJ diode-related design and optimizations. It should also be noted that although we use p-NiO as the representative p-type material, this work can still offer some general guidance about Ga_2O_3 diodes by replacing the NiO with other ultra-wide band gap p-type materials.

2. Simulation Methodology

Figure 1 depicts the schematic cross-sectional images of the vertical Ga_2O_3 diodes with the incorporation of p-NiO, namely SBD without p-NiO, HJ-PN diode, SBD with p-NiO GRs, and HJBS diode. All diodes possess a substrate doping concentration of 1×10^{19} cm^{-3} and the epi-layer has a doping concentration of 1×10^{16} cm^{-3} at a thickness of 5 μm, 10 μm and 15 μm. Various drift layer thicknesses (L) are used for evaluating the compromise between $R_{on,sp}$ and BV. All the p-NiO layer is with a thickness of 0.5 μm and the initial doping concentration is set to be 1×10^{18} cm^{-3}. For the diode architecture and performance optimizations, various p-NiO doping concentrations are considered and compared. For Ga_2O_3 SBDs with p-NiO GRs and HJBS diodes with various p-NiO, widths (W) and spacings (S) are also investigated.

Sentaurus TCAD device simulator from Synopsys was used to investigate device performances by considering different geometry and architecture. In the simulation, the electron mobility of Ga_2O_3 at room temperature is adjusted to be 200 cm^2/Vs due to the low doping concentration of 1×10^{16} cm^{-3}, and the remaining Ga_2O_3 parameters provided by the existing literature are shown in Table 1. At present, there are relatively few reports on NiO materials, so that the detailed simulation parameters of NiO materials are not provided by TCAD. In this paper, the NiO parameters are obtained according to the existing literature, which is summarized in Table 1.

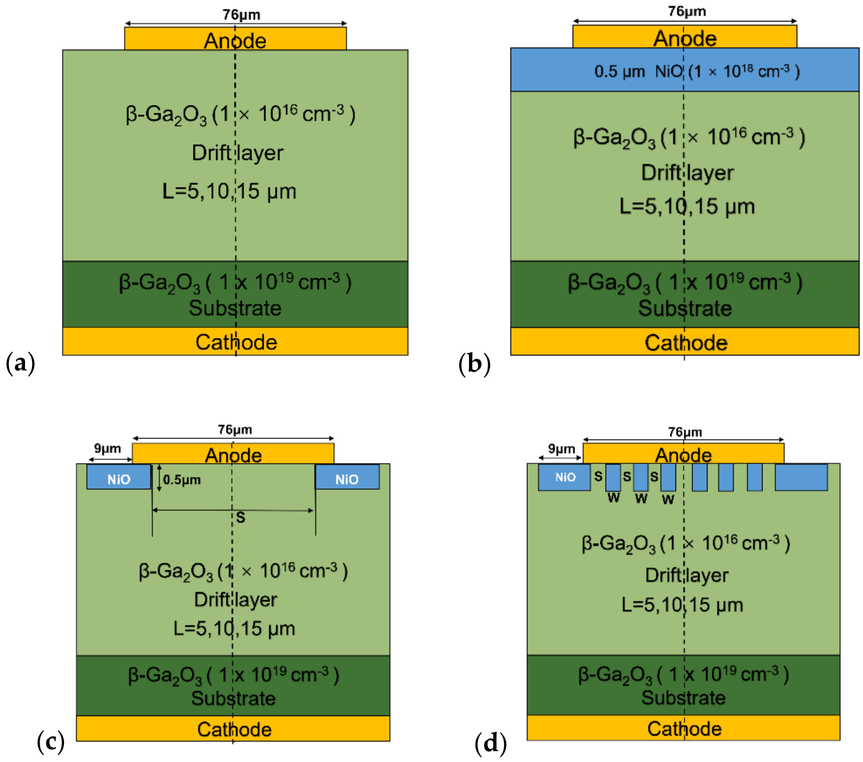

Figure 1. Schematic of the vertical NiO/Ga^2O^3 diode; (**a**) SBD without p-NiO, (**b**) HJ-PN diode, (**c**) SBD with GRs, (**d**) HJBS diode.

Table 1. Material parameters used for simulation.

Material	Ga_2O_3	NiO
Band gap (eV)	4.85 [1]	4 [22]
Electron affinity (eV)	3.9 [1]	1.8 [17]
Effective electron mass	0.28 [24]	-
Relative dielectric constant	10 [1]	11.8 [25]
Effective hole mass	-	6
Room-temperature electron mobility (cm^2/V s)	200	-
Room-temperature hole mobility (cm^2/V s)	-	0.5 [16]
Saturation electron velocity (cm/s)	2×10^7 [1]	-
Critical electric field (MV/cm)	8 [1]	4.8–6.2

The workfunction value of Schottky contact is 5.1 eV. In order to capture the accurate results, the following models are used: HighFieldSaturation model, SRH recombination model, thermionic current model, and band gap narrowing model. Accurate incomplete ionization parameters are currently unknow for NiO and Ga_2O_3. Thus, we assume that the dopants are completely ionized. Due to the lack of parameters of doping concentration model for NiO mobility, the experiment ignores the effect of doping concentration on mobility, and sets a fixed hole mobility of NiO (0.5 cm^2/V s). Breakdown simulations consider the impact ionization model based on the Chynoweth law with critical electrical field values of 8 MV/cm for Ga_2O_3. The critical breakdown electrical field of NiO is currently unclear, but it can be estimated from the band gap of NiO. According to the relationship between band gap and breakdown field in all semiconductors [26],

$$\varepsilon_c = 1.73 \times 10^5 (E_G)^{2.5}$$

It can be calculated that the breakdown field of NiO is between 4.8–6.2 MV/cm. For Schottky contact, an important injection mechanism is tunneling through the steep and thin

Schottky barrier. Thus, the electron tunneling model should be activated at the top of the Schottky contact. As for fabricated Ga_2O_3 devices, the off-state leakage current is orders of magnitude higher than the simulated off-state leakage current. This is due to impurities, defects, and traps in Ga_2O_3 and to background radiation. An equivalent background carrier generation is simulated through the Constant Carrier Generation model.

In order to verify the rationality of the simulation model, we simulated the structure of the reference (see Figure 2a, PN_ref) [16], and the current-voltage curves obtained are shown in Figure 2b. As shown in Table 2, the turn-on voltage (V_{on}), $R_{on,sp}$ as well as breakdown voltage (BV), is in good agreement with the reported results in the reference [16].

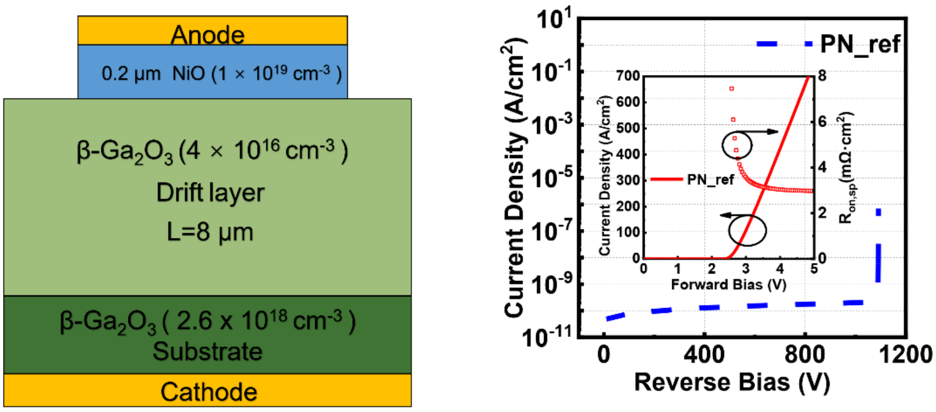

(**a**) (**b**)

Figure 2. (**a**) Schematic of the vertical NiO/Ga^2O^3 PN_ref and (**b**) simulated forward J-V characteristics and reverse J-V characteristics of the vertical NiO/Ga^2O^3 PN_ref.

Table 2. The device properties comparison between TCAD simulation and experimental results.

Device Properties	TCAD Simulation Results	Experimental Results of PN_ref
V_{on} (V)	2.4	2.4
$R_{on,sp}$ ($m\Omega \cdot cm^2$)	3.0	3.5
BV (V)	1091	1059

3. Results and Discussion

3.1. HJ PN Diode

One benefit of embracing the HJ-PN structure is that the V_{on} can be reduced by minimizing the band offset and hence improve the rectifying efficiency during power switching application. Figure 3a,b shows the forward and reverse linear-scaled J-V characteristics of the p-NiO/ Ga_2O_3 HJ-PN diodes with different drift layer thicknesses. The turn-on voltage (V_{on}) of the HJ-PN with a drift layer thickness of 5 μm, 10 μm, and 15 μm is extracted to be 2.35 V when the forward current density is defined at 1 A/cm^2. This low V_{on} is around 2 V lower when compared with the Ga_2O_3 PN homo-junction. Figure 3a shows the $R_{on,sp}$ of p-NiO/Ga_2O_3 HJ-PN diodes increases as the thickness of the drift layer increases. The $R_{on,sp}$ of HJ-PN diode is extracted to be 2.0 m$\Omega \cdot$cm^2, 3.2 m$\Omega \cdot$cm^2, and 4.3 m$\Omega \cdot$cm^2 for the 5 μm, 10 μm, and 15 μm drift layer thicknesses, respectively. The reverse leakage current of HJ-PN diode reaches 1 A/cm^2 at a reverse bias of 2500 V, 4465 V, and 5705 V for 5 μm, 10 μm, and 15 μm drift layer thicknesses, respectively. Figure 4 shows the electrical field distribution of the p-NiO/Ga_2O_3 HJ-PN diode with various drift layer thicknesses at a reverse bias of 3000 V. The peak electrical field of PN is located at the interface of HJ-PN, as can be seen in the electrical field distribution along the cutline, shown in Figure 4d. Since the electrical field within the NiO layer is smaller than that of Ga_2O_3, the doping concentration of NiO should be higher than that of Ga_2O_3 so that the depletion region of the HJ-PN extends toward Ga_2O_3 as much as possible. Thus, the increase in the thickness of the drift layer makes the width of the depletion region widened, and the peak electrical field decreases, rendering as the improvement of the BV. In summary, increasing the thickness of the drift layer will not change the V_{on}, but it will increase the $R_{on,sp}$ and increase the BV. The optimized BV/$R_{on,sp}$ is simulated to be 5705 V/4.3 mΩ·cm^2, translating to a PFOM = BV^2/$R_{on,sp}$ = 7.57 GW/cm^2.

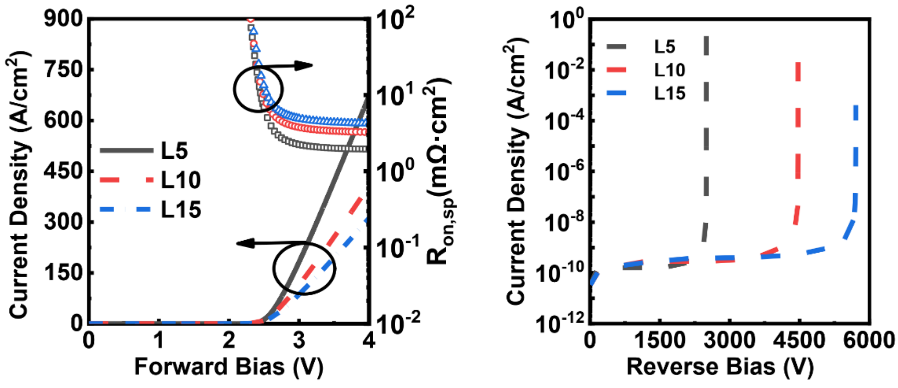

(**a**) (**b**)

Figure 3. (**a**) Forward J-V characteristics and Ron,sp–Forward V (**b**) reverse J-V characteristics of p-NiO/Ga_2O_3 with 5 µm, 10 µm, and 15 µm drift layer thicknesses.

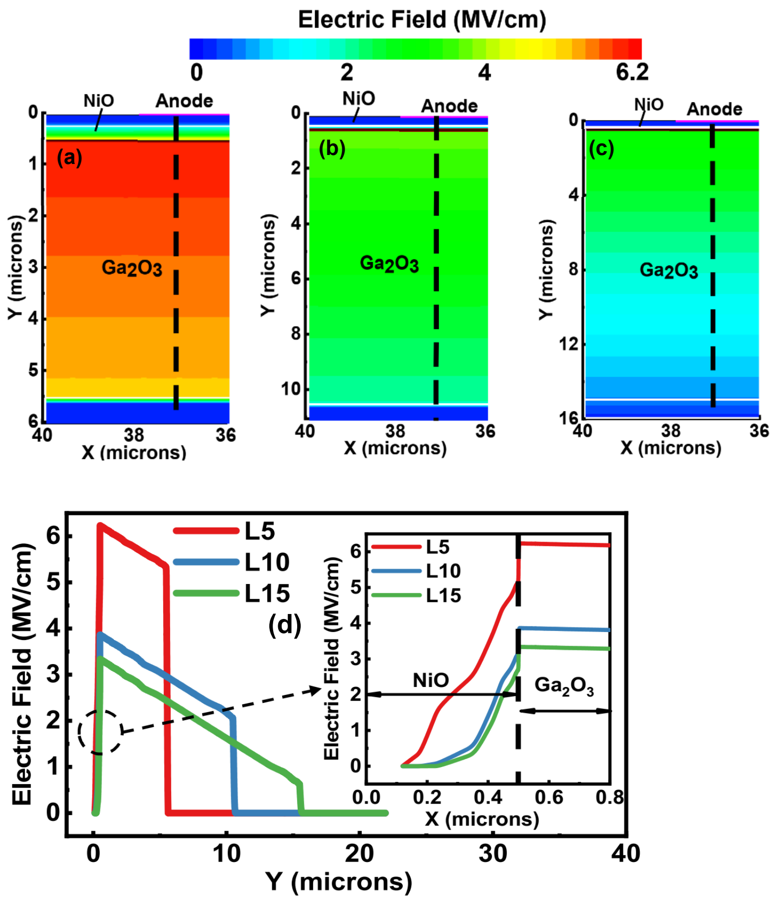

Figure 4. 2D electrical field distribution in HJ-PN diode with (**a**) 5 µm, (**b**) 10 µm, and (**c**) 15 µm drift layer thicknesses at a reverse bias of 3000 V. (**d**) Electrical field versus position for HJ-PN with 5 µm, 10 µm, and 15 µm drift layer thicknesses at −3000 V along the cutlines shown in the contour plots.

3.2. SBD with GRs

The Ga_2O_3 SBD with different width of p-NiO GRs and the one without GR are simulated for comparison, where the doping concentration of the p-NiO is 1×18 cm^{-3} and the drift layer thickness is initially set to be 10 μm. The forward and reverse J-V characteristics are summarized in Figure 5a,b. The V_{on} of the Ga_2O_3 SBD with various width of p-NiO GRs and the one with no GR are all around 1.1 V. The $R_{on,sp}$ of SBD with GRs is extracted to be 2.9 mΩ·cm^2, 3.4 mΩ·cm^2, 6.4 mΩ·cm^2, and 9.0 mΩ·cm^2 for the 0 μm, 22 μm, 37 μm, and 42 μm GR width, respectively. Obviously, as the width of GR increases inward, the V_{on} will not change, while the $R_{on,sp}$ increases. In SBD with GRs, the Schottky contact is turned on first, which causes the V_{on} of the SBD with GRs not likely to be affected by the width of the GR. As the width of the GR increases, the part of the Schottky contact becomes smaller, which leads to a decrease in the current density of the diode and an increase in the $R_{on,sp}$. The BV of SBD with different widths of the GR is 1748 V and it is greater than that of SBD with BV = 900 V. It should be noted that with the increase of GR width W, the reverse leakage current of SBD with GRs decreases, which is much smaller than that of SBD, as shown in Figure 5b.

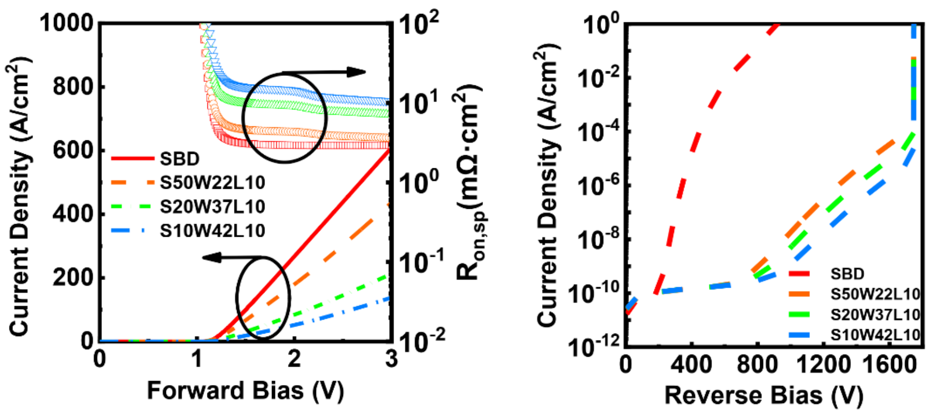

(**a**) (**b**)

Figure 5. (**a**) Forward J-V characteristics and $R_{on,sp}$ vs. forward bias and (**b**) reverse J-V characteristics of the Ga_2O_3 SBD with different width (W), spacing (S) of GRs and the one with no GR, at a p-NiO doping concentration of 1×18 cm^{-3} and a drift layer thickness (L) of 10 μm.

When the doping concentration of NiO is taken to be 1×10^{18} cm^{-3} and the anode bias is imposed by −1000 V, the electrical field profiles of the Ga_2O_3 SBD with no GR and the one with GRs are shown in Figure 6a,b, respectively. The maximum electrical field of SBD is 6.74 MV/cm at the edge of the anode, while the maximum electric field of SBD with GRs is 4.36 MV/cm at the edge of GR, which is far away from the anode edge. Although the critical electrical field of NiO is smaller than that of Ga_2O_3, due to the existence of GR, the maximum electrical field of SBD shifts from the edge of the anode to the edge of the GR, thereby effectively alleviating the crowding effect of the electrical field at the edge of the anode, and hence enhancing the BV.

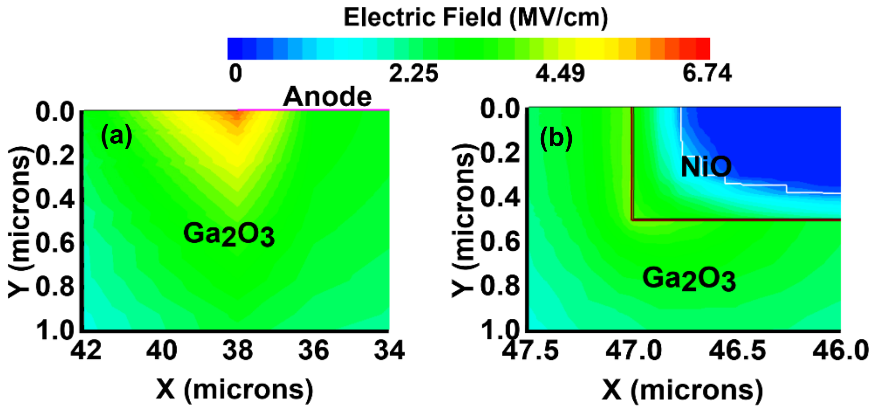

Figure 6. Electric field distribution in SBD with (**a**) no GR (**b**) GR at a reverse bias voltage of 1000 V. The doping concentration of the NiO is 1×10^{18} cm^{-3}, the width of GR is 42 μm, and the drift layer thicknesses is set to be 10 μm.

The relationship between the width of GR and the reverse leakage current can be explained by electron barrier tunneling. The tunneling of the electron barrier under the anodes of SBD with no GR and GRs is shown in Figure 7a,b, respectively. The electron barrier tunneling of SBD with no GR mainly occurs at the anode edge. Introducing the NiO GR avoids the electron barrier tunneling at the anode edge, thereby reducing the reverse leakage current. When the width of the GR decreases, the tunneling probability of the electron barrier under the anode of the SBD with GRs remains unchanged, as shown in Figure 7c, but as the width of the GR becomes wider, the tunneling path of the electron barrier becomes shorter, which makes the reverse leakage current to be reduced.

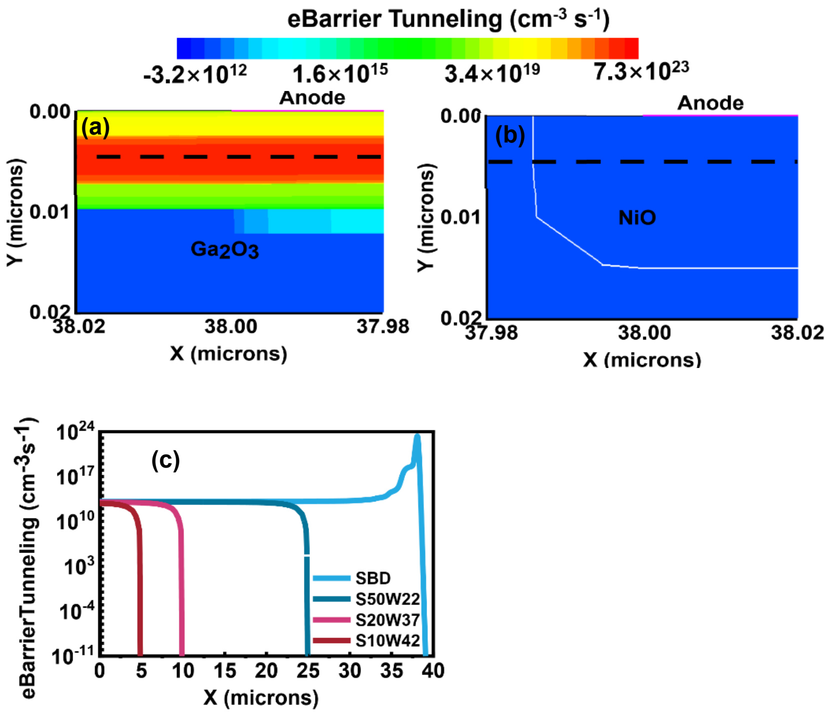

Figure 7. Electron barrier tunneling across the Schottky interface for Ga_2O_3 SBD with a 10-μm thick, 10^{16} cm^{-3} with (**a**) no GR, and (**b**) GRs at reverse bias of 500 V, when the doping concentration of the NiO is 1×10^{18} cm^{-3}. (**c**) Electron barrier tunneling versus position for SBD with no GR and the GR width of 22 μm, 37 μm, 42 μm, at −500 V along the cutlines shown in the contour plots.

The change in the drift layer thickness of the Ga_2O_3 SBD with GRs affects the forward and reverse J-V characteristics as given by Figure 8a,b. The V_{on} of the SBD with various thicknesses of the drift layer at a 42-µm-width GR (N_A = 1 × 18 cm^{-3}) is still 1.1 V. The $R_{on,sp}$ of SBD with GRs is extracted to be 7.6 mΩ·cm^2, 10.4 mΩ·cm^2, and 11.23 mΩ·cm^2 for the 5 µm, 10 µm, and 15 µm drift layer thickness, respectively. Thus, in the SBD with GRs different thickness of the drift layer does not affect their V_{on}, but the $R_{on,sp}$ increases as the drift layer thickness is increased. The BV is determined to be 1231 V, 1747 V, and 1948 V for 5 µm,10 µm, and15 µm drift layer thickness, respectively. The change in the drift layer thickness of the Ga_2O_3 SBD with GRs also modified the electrical field distribution. As the thickness of the GR drift layer increases, the peak electrical field of the SBD with GRs at a reverse bias of 2000 V decreases from 7.72 MV/cm to 5.8 MV/cm, as shown in Figure 9d. When the thickness of the drift layer increases from 5 µm to 10 µm, the peak electrical field reduces from 7.72 MV/cm to 6.11 MV/cm; the peak electrical field is reduced from 6.11 MV/cm to 5.8 MV/cm when the thickness of drift layer increases from 10 µm to 15 µm, as depicted in Figure 9a–c. For the reverse leakage current, increasing the thickness of the drift layer from 5 µm to 10 µm can effectively reduce the leakage current to a large extent. When the thickness of the drift layer exceeds 10 µm, the capability to reduce the leakage current will be weakened.

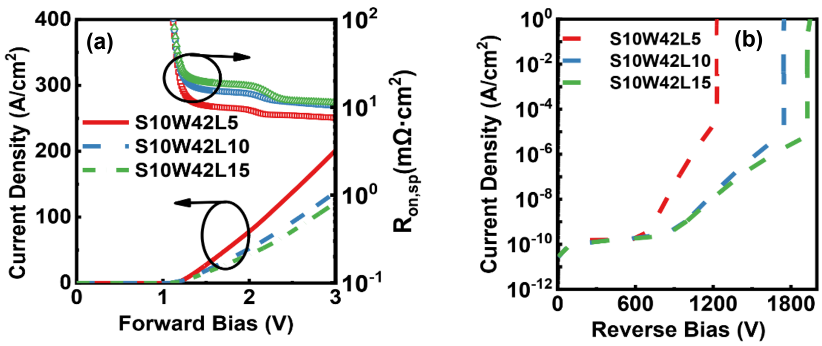

Figure 8. (**a**) Forward J-V and (**b**) reverse J-V characteristics of the Ga_2O_3 SBD with 5 µm, 10 µm, and 15 µm drift layer thicknesses, when the width of GR is 42 µm and the doping concentration of GR is 1 × 10^{18} cm^{-3}.

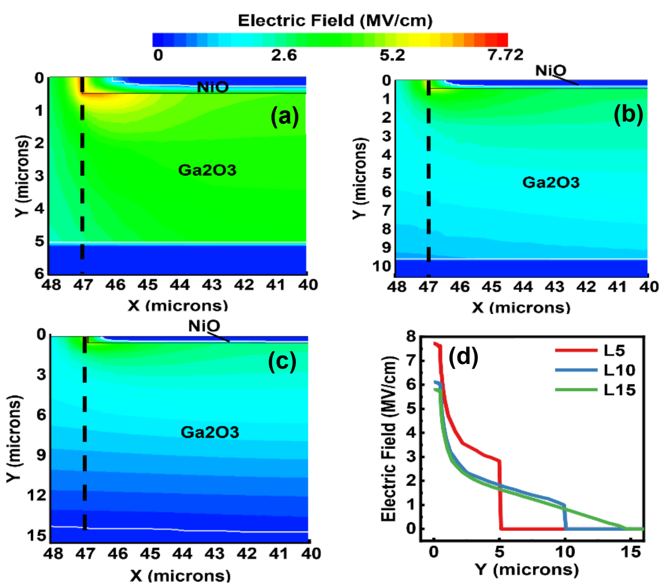

Figure 9. 2D electric field distribution in SBD with the 42-µm-width NiO for (**a**) 5 µm, (**b**) 10 µm, and (**c**) 15 µm drift layer thicknesses at reverse bias of 2000 V, respectively. (**d**) Electrical field versus position for SBD with 5 µm, 10 µm, and 15 µm drift layer thicknesses at −2000 V along the cutlines shown in the contour plots.

Doping concentration of the p-NiO GR is a critical parameter that can affect the electrical characteristics of SBD. The relationship between the doping concentration of the 12-μm-width GR and the J-V characteristics of SBD with the 10-μm-thick drift layer is shown in Figure 10a,b. The $R_{on,sp}$ of the SBD with the 12-μm-width GR is extracted to be 3.19 mΩ·cm^2, 3.16 mΩ·cm^2, 3.07 mΩ·cm^2, 2.97 mΩ·cm^2, 2.62 mΩ·cm^2, 2.55 mΩ·cm^2 for 1×10^{16} cm^{-3}, 1×10^{17} cm^{-3}, 4×10^{17} cm^{-3}, 1×10^{18} cm^{-3}, 1×10^{19} cm^{-3}, 7×10^{19} cm^{-3} NiO doping concentration, respectively. The maximum BV of Ga_2O_3 SBD with GR width of 12 μm at GR doping concentration of 4×10^{17} is 3006 V, as shown in Figure 10b,c. The V_{on} of the Ga_2O_3 SBD with GRs is still 1.1 V, and the $R_{on,sp}$ will decrease as the NiO doping concentration increases, as shown in Figure 10a. We have also simulated the BV of Ga_2O_3 SBD with 12-μm-width GRs under the drift layer thickness of 5 μm, 10 μm, and 15 μm, as a function of NiO doping, as shown in Figure 10b. When the doping concentration of the p-NiO GRs is between 1×10^{16}–4×10^{17} cm^{-3}, the BV increases with the increase of doping concentration. On the contrary, when the doping concentration of GR is between 4×10^{17}–1×10^{18} cm^{-3}, the BV of Ga_2O_3 SBD with GR decreases with the increase of doping concentration. Finally, when the doping concentration of GR is greater than 1×10^{18} cm^{-3}, the BV of Ga_2O_3 SBD with GRs increases with the increase of doping concentration. The simulated BV versus p-NiO GR doping concentration is shown in Figure 10c. This change is caused by the transfer of the breakdown point due to the different doping concentration of GR. The breakdown point of SBD with GRs doped with different concentrations changes from the anode edge (1×10^{16} cm^{-3}–1×10^{17} cm^{-3}) to the junction of p-type region and n-type region below the anode (3×10^{17}–4×10^{17} cm^{-3}) and then to the edge of p-ring (5×10^{17}–1×10^{20} cm^{-3}) with the increase of doping concentration. Considering that the BV of SBD with different GR widths remains the same, the maximum BV is 2017 V, 3006 V, and 3597 V for 5 μm, 10 μm, and 15 μm drift layer thickness, respectively.

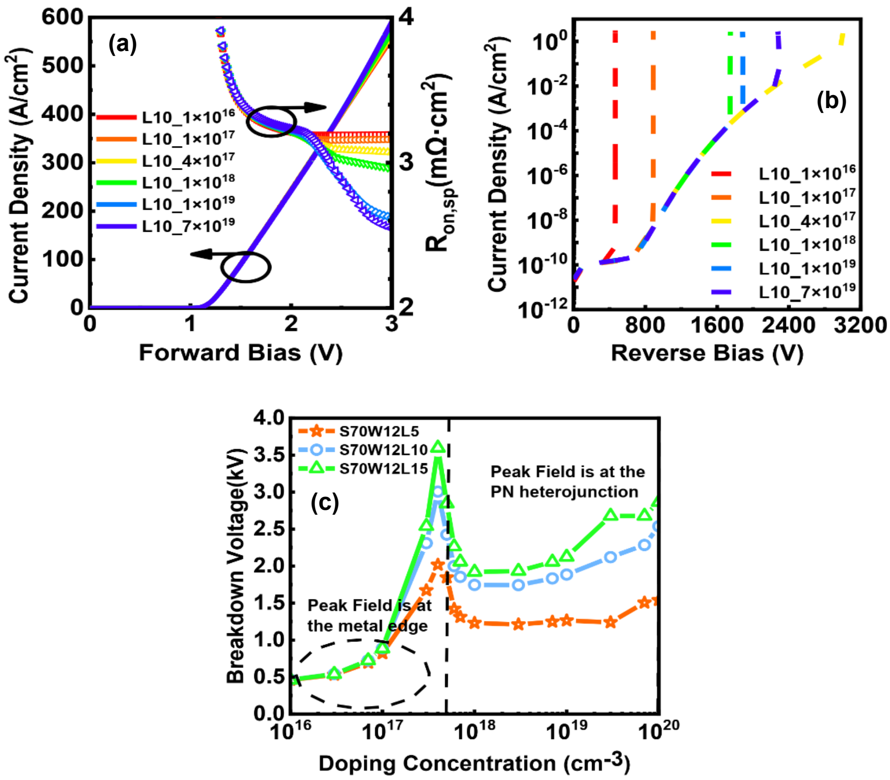

Figure 10. (**a**) Forward J-V and (**b**) reverse J-V characteristics of the Ga_2O_3 SBD with different doping concentrations of the p-NiO GRs, when the width of GR is 12 μm. (**c**) Breakdown voltage versus p-NiO GR doping concentration with 12 μm of GR width for different drift layer thicknesses.

In summary, the forward electrical characteristics and reverse leakage current of the SBD with GRs are related to the width of the GR and the thickness of the drift layer, and the doping concentration of the GR, while its BV is related to the doping concentration of the GR and the thickness of the drift layer. Proper doping concentration of GRs and drift layer thickness can make SBD with GRs obtain ultra-high BV while keeping a small $R_{on,sp}$. The optimized BV/$R_{on,sp}$ is simulated to be 3006 V/3.07 mΩ·cm^2, translating to a PFOM = $BV^2/R_{on,sp}$ = 2.94 GW/cm^2.

3.3. HJBS Diode

JBS diode is a typical SBD structure, which is used to increase BV and reduce reverse leakage current while maintaining a low V_{on}. In this part, we explore the use of p-NiO as the p-type material to construct Ga_2O_3 HJBS. There are 6 fins under the anode and the drift layer thickness is 10 µm. Considering the best performance of Ga_2O_3 SBD with NiO GRs when the NiO doping concentration is 4×10^{17} cm^{-3}, we compare HJBS with NiO doping concentration of 1×10^{18} cm^{-3} and 4×10^{17} cm^{-3}. Meanwhile, we simulated three HJBS diode configurations with different fin widths and spacings: (1) the width of NiO fin is 8 µm, the Ga_2O_3 space is 2 µm; (2) the width of NiO fin is 8 µm, the Ga_2O_3 space is 3 µm; (3) the width of NiO fin is 5 µm, the Ga_2O_3 space is 6 µm.

The forward J-V characteristics of HJBS are affected by the doping concentration of the p-type region and the total width of NiO, as shown in Figure 11a. The V_{on} of the HJBS with different fin width, spacing, and doping concentration is still 1.1 V, which is the same as the V_{on} of SBD with a 10-µm-thick drift layer. The $R_{on,sp}$ of HJBS with the NiO doping concentration of 1×10^{18} cm^{-3} is extracted to be 3.32 mΩ·cm^2, 3.29 mΩ·cm^2, and 2.99 mΩ·cm^2 for the 2 µm, 3 µm, and 5 µm Ga_2O_3 fin space width, respectively. The $R_{on,sp}$ of HJBS with the NiO doping concentration of 4×10^{17} cm^{-3} is extracted to be 3.56 mΩ·cm^2, 3.46 mΩ·cm^2, and 3.06 mΩ·cm^2 for the 2 µm, 3 µm, and 5 µm Ga_2O_3 fin space width, respectively. The $R_{on,sp}$ of HJBS diode increases with the increase of the total width of NiO which is higher than the $R_{on,sp}$ of SBD. This result shows that the forward characteristic of HJBS is related to the total width of p-NiO and the doping concentration of p-NiO.

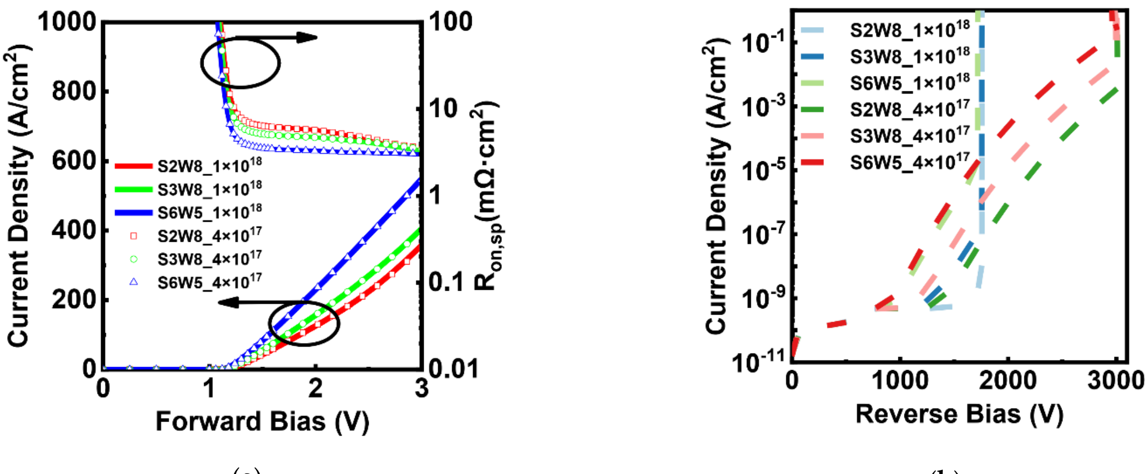

Figure 11. (**a**) Forward J-V characteristics and $R_{on,sp}$ vs. forward bias (**b**) reverse J-V characteristics of the p-NiO/Ga_2O_3 HJBS with different width, space, and doping concentration of p-NiO, when the thickness of drift layer is 10 µm.

Figure 11b shows the reverse J-V characteristics of different p-NiO width, space, and p-NiO doping concentration. The BV of HJBS diode is 1757 V and 3004 V for 1×10^{18} cm^{-3} and 4×10^{17} cm^{-3} p-NiO doping concentration, respectively. Obviously, the BV of the HJBS diode is related to the doping concentration of p-NiO, and less likely to be related with the total width of p-NiO. The most important point is that the BV of HJBS diode will be approximately the same as the SBD with p-NiO GRs when their doping concentration remains the same. Thus, the maximum BV of HJBS can be obtained when the p-NiO doping concentration is 4×10^{17} cm^{-3}. When the p-NiO doping concentration is 1×10^{18} cm^{-3}, the peak electrical field is on the side of the HJ-PN, which is away from the anode edge. In contrast, when the NiO doping concentration is 4×10^{17} cm^{-3}, the peak electrical field is located at the PN junction below the anode, as shown in Figure 12. At the same time, the maximum electric field is reduced from 7.53 MV/cm to 5 MV/cm.

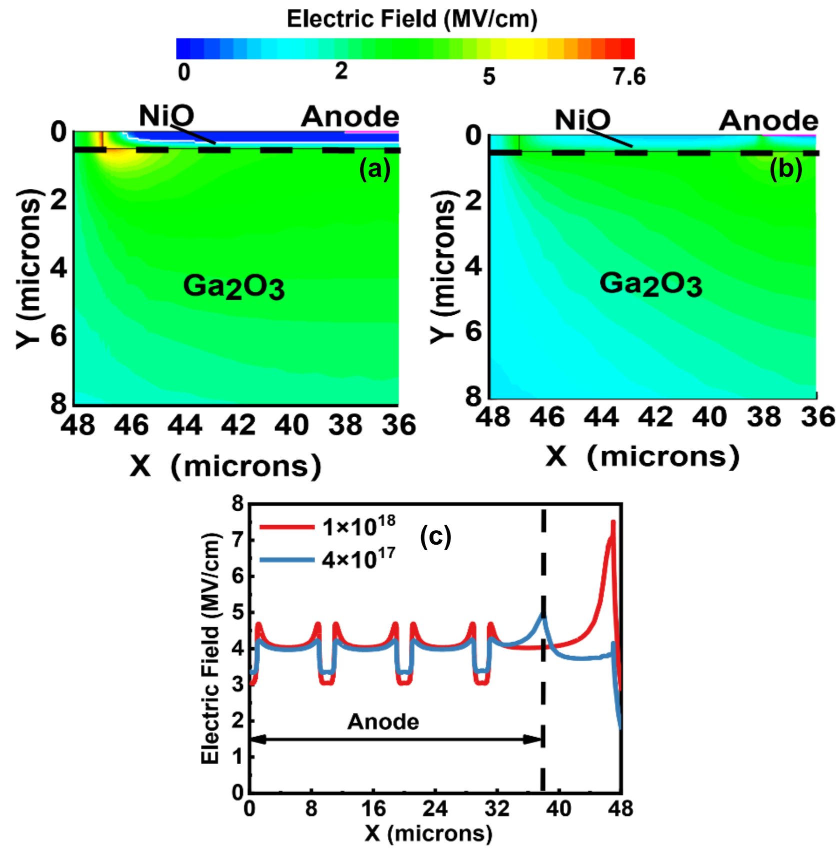

Figure 12. Electric field distribution in HJBS diode with the 8-µm-width fin, the 2-µm-width space, the doping concentration of (**a**) 1×10^{18} cm^{-3} and (**b**) 4×10^{17} cm^{-3} at reverse bias of −3000 V. (**c**) Electric field versus position for HJBS diode along the cutline shown in the contour plots.

The doping concentration and the total width of p-NiO are found to affect the reverse leakage current of the HJBS. The reverse leakage current will decrease with the increase of the total width of NiO. The low doping concentration of p-NiO leads to a slightly higher leakage current, as shown in Figure 11b. The reason for the change in leakage current is that as the doping concentration of p-NiO increases, the electron concentration in the depletion region under the anode decreases. Therefore, fewer electrons can pass through the barrier, as shown in Figure 13. Among all the HJBS diodes described above, the correlation between the forward characteristics with p-NiO doping concentration and the total width of p-NiO underneath the anode is similar to SBD with NiO GRs, and the BV of HJBS diodes are almost the same as SBD with p-NiO GRs at the same p-NiO doping concentration. HJBS has a great potential to suppress leakage current, and the capability to suppress reverse leakage current is not only related to the total length of NiO, but also to the doping concentration of p-NiO. The optimized BV/$R_{on,sp}$ is simulated to be 3004 V/3.06 mΩ·cm^2, translating to a PFOM = $BV^2/R_{on,sp}$ = 2.95 GW/cm^2.

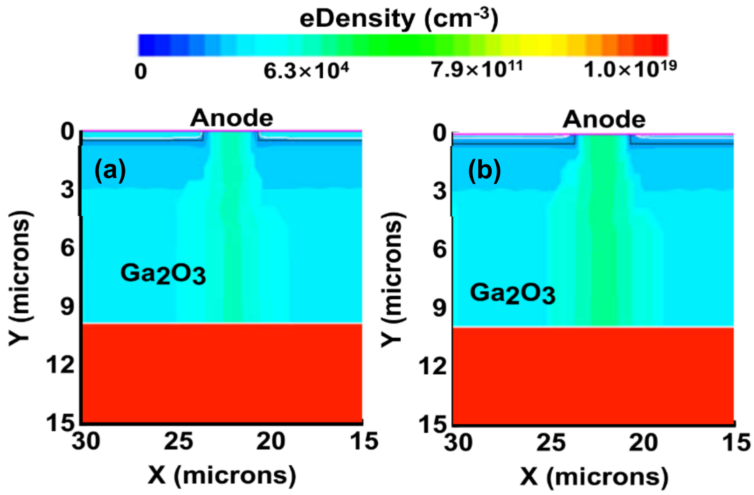

Figure 13. Electron density in HJBS diode with the 8-μm-width of p-NiO fin, 3-μm-width of Ga_2O_3 space at a reverse bias of −1500 V and p-NiO doping concentration of (**a**) 1×10^{18} cm^{-3} and (**b**) 4×10^{17} cm^{-3}.

4. Conclusions

In summary, p-NiO/Ga_2O_3 diode performances were studied by using a detailed device simulation. Figure 14 summarizes some of the design recommendations. The HJ-PN diodes without any field-plate or other electric field managements can obtain a maximum BV of 5705 at a 15 μm drift layer thickness. For Ga_2O_3 SBD with p-NiO GRs and HJBS diodes, the V_{on} is 1.1 V and the wider the total width of the p-NiO, the larger $R_{on,sp}$ with a smaller reverse leakage current will be, while maintaining the same p-type p-NiO doping concentration. When the total width of the p-NiO remains a constant, suitable doping concentration of p-NiO can effectively improve the BV. In this article, when the p-NiO doping concentration is 4×10^{17} cm^{-3}, a maximum BV can be obtained. Another way to increase the BV is to increase the thickness of the drift layer. Ga_2O_3 SBD with p-NiO GRs and HJBS diode has the same BV under the same p-NiO doping concentration. The simulated BV and P-FOM are far beyond the performance of the state-of-the-art Ga_2O_3 power diode, showing the great promise of combining p-NiO in the Ga_2O_3 power electronics.

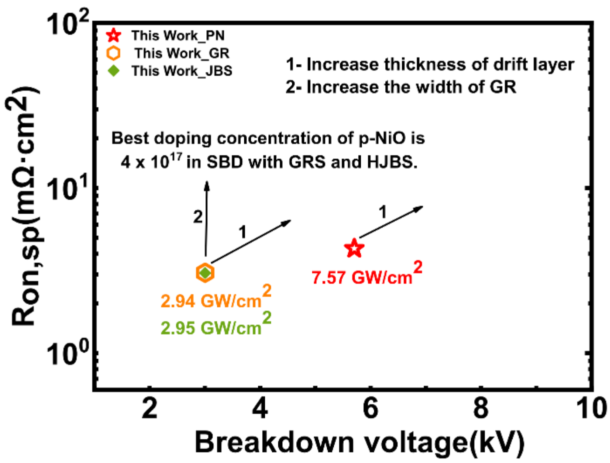

Figure 14. DC Ron,sp–BV benchmark comparison some design methods.

Author Contributions: H.Z. designed the study and wrote the paper; S.Z. performed the research and collected the data; formal analysis, H.Z., Z.L., J.Z. (Jinfeng Zhang), Q.F. and S.X.; resource, J.Z. (Jincheng Zhang) and Y.H. All authors have read and agreed to the published version of the manuscript.

Funding: This work is supported in part by National Natural Science Foundation of China under Grant No. 62004147 and Wuhu and Xidian University special fund for industry university research cooperation under Grant No. XWYCXY-012020011, in part by the Fundamental Research Funds for the Central Universities and the Innovation Fund of Xidian University.

Conflicts of Interest: The authors declare no conflict of interest.

References

1. Pearton, S.J.; Yang, J.; Cary, P.H.; Ren, F.; Mastro, M.A. A review of Ga_2O_3 materials, processing, and devices. *Appl. Phys. Rev.* **2018**, *5*, 011301. [CrossRef]
2. Higashiwaki, M.; Jessen, G.H. Guest Editorial: The dawn of gallium oxide microelectronics. *Appl. Phys. Lett.* **2018**, *112*, 060401. [CrossRef]
3. Kuramata, A.; Koshi, K.; Watanabe, S.; Yamaoka, Y.; Masui, T.; Yamakoshi, S. High-quality β-Ga2O3 single crystals grown by edge-defined film-fed growth. *Jpn. J. Appl. Phys.* **2016**, *55*, 1202A2. [CrossRef]
4. Galazka, Z.; Irmscher, K.; Uecker, R.; Bertram, R.; Pietsch, M.; Kwasniewski, A.; Naumann, M.; Schulz, T.; Schewski, R.; Klimm, D. On the bulk β-Ga2O3 single crystals grown by the Czochralski method. *J. Cryst. Growth* **2014**, *404*, 184–191. [CrossRef]
5. Irmscher, K.; Galazka, Z.; Pietsch, M.; Uecker, R.; Fornari, R. Electrical properties of β-Ga2O3 single crystals grown by the Czochralski method. *J. Appl. Phys.* **2011**, *110*, A316–A350. [CrossRef]
6. Baliga, B.J. Power semiconductor device figure of merit for high-frequency applications. *IEEE Electron. Device Lett.* **1989**, *10*, 455–457. [CrossRef]
7. Konishi, K.; Goto, K.; Murakami, H.; Kumagai, Y.; Kuramata, A.; Yamakoshi, S.; Higashiwaki, M. 1-kV vertical Ga2O3 field-plated Schottky barrier diodes. *Appl. Phys. Lett.* **2017**, *110*, 103506. [CrossRef]
8. Kumar, N.; Joishi, C.; Xia, Z.; Rajan, S.; Kumar, S. Electrothermal Characteristics of Delta-Doped beta-Ga2O3 Metal-Semiconductor Field-Effect Transistors. *IEEE Trans. Electron. Devices* **2019**, *66*, 5360–5366. [CrossRef]
9. Sharma, S.; Zeng, K.; Saha, S.; Singisetti, U. Field-Plated Lateral Ga2O3 MOSFETs with Polymer Passivation and 8.03 kV Breakdown Voltage. *IEEE Electron. Device Lett.* **2020**, *41*, 836–839. [CrossRef]
10. Li, W.; Nomoto, K.; Hu, Z.; Nakamura, T.; Xing, H.G. Single and multi-fin normally-off Ga2O3 vertical transistors with a breakdown voltage over 2.6 kV. In Proceedings of the 2019 IEEE International Electron Devices Meeting (IEDM), San Francisco, CA, USA, 7–11 December 2019.
11. Hu, Z.; Hong, Z.; Qian, F.; Zhang, J.; Zhang, C.; Dang, K.; Cai, Y.; Feng, Z.; Gao, Y.; Kang, X. Field-Plated Lateral β-Ga2O3 Schottky Barrier Diode with High Reverse Blocking Voltage of More Than 3 kV and High DC Power Figure-of-Merit of 500 MW/cm^2. *IEEE Electron. Device Lett.* **2018**, *39*, 1564–1567. [CrossRef]
12. Zhou, H.; Yan, Q.L.; Zhang, J.C.; Lv, Y.J.; Liu, Z.H. High-Performance Vertical β-Ga2O3 Schottky Barrier Diode With Implanted Edge Termination. *IEEE Electron. Device Lett.* **2019**, *40*, 1788–1791. [CrossRef]
13. Li, W.; Nomoto, K.; Hu, Z.; Jena, D.; Xing, H.G. Field-Plated Ga2O3 Trench Schottky Barrier Diodes with a BV2/Ron,sp of up to 0.95 GW/cm2. *IEEE Electron. Device Lett.* **2019**, *41*, 107–110. [CrossRef]
14. Zhou, H.; Zhang, J.; Zhang, C.; Feng, Q.; Hao, Y. A review of the most recent progresses of state-of-art gallium oxide power devices. *J. Semicond.* **2019**, *40*, 011803. [CrossRef]
15. Varley, J.B.; Janotti, A.; Franchini, C.; Van de Walle, C.G. Role of self-trapping in luminescence and p-type conductivity of wide-band-gap oxides. *Phys. Rev. B Condens. Matter Mater. Phys.* **2012**, *85*, 081109. [CrossRef]
16. Lu, X.; Zhou, X.; Jiang, H.; Ng, K.r.W.; Wang, G. 1-kV sputtered p-NiO/n-Ga_2O_3 heterojunction diodes with an ultra-low leakage current below 1 $\mu A/cm^2$. *IEEE Electron. Device Lett.* **2020**, *41*, 449–452. [CrossRef]
17. Gong, H.H.; Chen, X.H.; Xu, Y.; Ren, F.F.; Ye, J.D. A 1.86-kV double-layered NiO/β-Ga_2O_3 vertical p-n heterojunction diode. *Appl. Phys. Lett.* **2020**, *117*, 22104. [CrossRef]
18. Kokubun, Y.; Kubo, S.; Nakagomi, S. All-oxide p–n heterojunction diodes comprising p-type NiO and n-type β-Ga_2O_3. *Appl. Phys. Express* **2016**, *9*, 091101. [CrossRef]
19. Watahiki, T.; Yu Da, Y.; Furukawa, A.; Yamamuka, M.; Takiguchi, Y.; Miyajima, S. Heterojunction p-Cu2O/n-Ga_2O_3 diode with high breakdown voltage. *Appl. Phys. Lett.* **2017**, *111*, 222104. [CrossRef]
20. Vera, F.; Schrebler, R.; Munoz, E.; Suarez, C.; Cury, P.; Gomez, H.; Cordova, R.; Marotti, R.; Dalchiele, E. Preparation and characterization of Eosin B- and Erythrosin J-sensitized nanostructured NiO thin film photocathodes. *Thin Solid Film.* **2005**, *490*, 182–188. [CrossRef]
21. Lu, Y.M.; Hwang, W.S.; Yang, J.S. Effects of substrate temperature on the resistivity of non-stoichiometric sputtered NiOx films. *Surf. Coat. Technol.* **2002**, *155*, 231–235. [CrossRef]
22. Tyagi, M.; Tomar, M.; Gupta, V. P-N Junction of NiO Thin Film for Photonic Devices. *IEEE Electron. Device Lett.* **2013**, *34*, 81–83. [CrossRef]

23. Yan, Q.; Gong, H.; Zhang, J.; Ye, J.; Hao, Y. β-Ga_2O_3 hetero-junction barrier Schottky diode with reverse leakage current modulation and BV2 /Ron,sp value of 0.93 GW/cm^2. *Appl. Phys. Lett.* **2021**, *118*, 122102. [CrossRef]
24. Nan, M.; Tanen, N.; Verma, A.; Zhi, G.; Luo, T.; Xing, H.; Jena, D. Intrinsic Electron Mobility Limits in beta-Ga_2O_3. *Appl. Phys. Lett.* **2016**, *109*, 212101.
25. Gielisse, P.J.; Plendl, J.N.; Mansur, L.C.; Marshall, R.; Smakula, A. Infrared Properties of NiO and CoO and Their Mixed Crystals. *J. Appl. Phys.* **1965**, *36*, 2446–2450. [CrossRef]
26. Hudgins, J.L.; Simin, G.S.; Santi, E.; Khan, M.A. An assessment of wide bandgap semiconductors for power devices. *IEEE Trans. Power Electron.* **2003**, *18*, 907–914. [CrossRef]